

STRUCTURE AND COLORS OF DIFFUSE EMISSION IN THE *SPITZER* GALACTIC FIRST LOOK SURVEY

JAMES G. INGALLS,¹ M.-A. MIVILLE-DESCHÊNES,² WILLIAM T. REACH,¹ A. NORIEGA-CRESPO,¹ SEAN J. CAREY,¹ F. BOULANGER,³
S. R. STOLOVY,¹ DEBORAH L. PADGETT,¹ M. J. BURGENDORF,¹ S. B. FAJARDO-ACOSTA,¹ W. J. GLACCUM,¹ G. HELOU,¹
D. W. HOARD,¹ J. KARR,¹ J. O'LINGER,¹ L. M. REBULL,¹ J. RHO,¹ J. R. STAUFFER,¹ AND S. WACHTER¹

Received 2004 April 5; accepted 2004 May 5

ABSTRACT

We investigate the density structure of the interstellar medium using new high-resolution maps of the 8, 24, and 70 μm surface brightness toward a molecular cloud in the Gum Nebula, made as part of the *Spitzer Space Telescope* Galactic First Look Survey. The maps are correlated with 100 μm images measured with *IRAS*. At 24 and 70 μm , the spatial power spectrum of surface brightness follows a power law with a spectral index of -3.5 . At 24 μm , the power-law behavior is remarkably consistent from the ~ 0.2 size of our maps down to the $\sim 5''$ spatial resolution. Thus, the structure of the 24 μm emission is self-similar even at milliparsec scales. The combined power spectrum produced from *Spitzer* 24 μm and *IRAS* 25 μm images is consistent with a change in the power-law exponent from -2.6 at spatial wavenumber $k \sim 2 \times 10^{-3} \text{ arcsec}^{-1}$ to -3.5 at $k \sim 4 \times 10^{-3} \text{ arcsec}^{-1}$. The decrease may be due to the transition from a two-dimensional to three-dimensional structure. Under this hypothesis, we estimate the thickness of the emitting medium to be 0.3 pc.

Subject headings: infrared: ISM — ISM: individual (DC 254.5–9.6, Gum Nebula) — ISM: structure — turbulence

1. INTRODUCTION

More than 50 years ago, astronomers began to reconsider the concept of an homogeneous density and velocity structure for the interstellar medium (ISM). The seminal lecture on astrophysical turbulence by Chandrasekhar (1949) marked the recognition that studies of the ISM were incomplete without knowledge of the physical and observational consequences of turbulence. The structure and the dynamics of the ISM critically affect its chemistry (Spaans 1996; Joulain et al. 1998; Röllig et al. 2002) and its star-formation capacity (see, for example, the review by MacLow & Klessen 2004). The ramifications of a turbulent velocity and density field for radiative transfer must be taken into account when interpreting spectral line and continuum observations of interstellar clouds (Padoan et al. 1998; Hegmann & Kegel 2000, 2003; Ossenkopf 2002; Juvela & Padoan 2003). Finally, knowledge of the structure of Milky Way interstellar matter is essential to the proper interpretation of extragalactic counts and measurements of the spatial distribution of the cosmic microwave background (Gautier et al. 1992).

The structural statistics of the ISM are self-similar on a wide range of scales, from hundreds of parsecs down to ~ 0.02 pc (Bensch et al. 2001). The angular power spectrum of two-dimensional images of interstellar emission and absorption derived using a variety of tracers yields a power law as a function of wavenumber k^β with the exponent ranging from $\beta \sim -3.6$ (Miville-Deschênes et al. 2003a) to $\beta \sim -2.5$ (Bensch et al. 2001; see also the review by Falgarone et al. 2004). Power spectral analysis of the far-infrared emission

from the Galactic cirrus results in the same range of values on angular scales of $1'$ and larger (Gautier et al. 1992; Herbstmeier et al. 1998).

The *Spitzer Space Telescope* allows us to extend the examination of turbulent density fields down to $\sim 5''$ scales. We present new high-resolution maps of the 8, 24, and 70 μm diffuse emission toward the Gum Nebula, made as part of the *Spitzer* Galactic First Look Survey (GLFS; see § 2). In § 3 we derive colors between the *Spitzer* and *Infrared Astronomical Satellite (IRAS)* bands and perform a power spectral analysis of the *Spitzer* images. For the 24 and 70 μm maps, we find power-law exponents similar to those derived from H I observations, with no detectable break at high wavenumbers down to spatial scales of ~ 0.01 pc. We discuss the implications of our results for interstellar structure in § 4.

2. OBSERVATIONS

2.1. The *Spitzer* Galactic First Look Survey

The new data that we analyze form part of the *Spitzer Space Telescope* (Werner et al. 2004) Galactic First Look Survey.⁴ We describe here observations made using the Infrared Array Camera (IRAC; Fazio et al. 2004) and Multiband Imaging Photometer for *Spitzer* (MIPS; Rieke et al. 2004) instruments aboard *Spitzer*. The IRAC observations (Program ID [PID] 104; *Spitzer* AOR 0006579712) were conducted on 2003 December 7, and the MIPS observations (PID 104; *Spitzer* AOR 0006578176) were conducted on 2003 December 9.

The surface brightness maps on which we have performed power spectral analysis are shown in Figure 1 (Plate 1). The images on the left side of the figure are the output of the automated post-Basic Calibrated Data (post-BCD) *Spitzer* calibration pipeline.⁵ For each of the three *Spitzer* bands considered in this study—IRAC 8 μm and MIPS 24 and 70 μm —

¹ *Spitzer* Science Center, California Institute of Technology, 1200 East California Boulevard, MC 220-6, Pasadena, CA 91125; offprint requests: ingalls@ipac.caltech.edu.

² Canadian Institute for Theoretical Astrophysics, 60 St. George Street, Toronto, ON M5S 3H8, Canada.

³ Institut d'Astrophysique Spatiale, Université Paris-Sud, bât. 121, F-91405, Orsay, France.

⁴ See <http://ssc.spitzer.caltech.edu/fls/galac>.

⁵ See <http://ssc.spitzer.caltech.edu/postbcd>.

we have analyzed slightly different fields, albeit with considerable overlap. There was a small mismatch in the observed IRAC and MIPS fields caused by a $\sim 2^\circ$ rotation of *Spitzer* between the two observation dates. We also truncated the $70\ \mu\text{m}$ mosaic, because of excessive noise in portions of the image.

Each of the examined regions are centered on Galactic coordinates $(l, b) = (254.5, -9.5)$ and cover a square of size $\sim 0.1\text{--}0.3$ (see Fig. 1) comprising less than 2% of the GFLS total sky coverage. This line of sight intersects a molecular cloud associated with the Gum Nebula, an expanding super-shell of radius $\sim 70\text{--}130$ pc (Yamaguchi et al. 1999). The CO gas associated with the *Spitzer* field has negative radial velocities, placing it on the near side of the bubble. Since the expansion center is at most 500 pc from the Sun (Woermann et al. 2001), we estimate a distance $d \sim 400$ pc to our field. The 24 and $70\ \mu\text{m}$ fields also include the object DC 254.5–9.6 from the optical catalog of southern dark clouds of Hartley et al. (1986).

Before estimating the power spectrum, the *Spitzer* images shown in the left column of Figure 1 were processed to remove point sources and instrumental noise. The emission from point sources was characterized and removed using the Star-Finder code written in IDL (Diolaiti et al. 2000a, 2000b). The images were then filtered to remove instrumental noise using a multiresolution wavelet technique (Starck & Murtagh 1998). The method required an estimate of the noise spatial response. Following Miville-Deschênes et al. (2003b), we used the uncertainty images automatically produced by the post-BCD pipeline to account for spatial variations in the noise. The right column of Figure 1 shows the left column images after point-source removal and noise filtering.

Power spectra for each of the images in Figure 1 were computed by squaring the amplitudes of the image Fourier transforms. Prior to transforming the images, the outer 5% of pixels were multiplied by a cosine taper. This apodization function minimized edge effects caused by our nonperiodic data. In Fourier wavenumber (k) space, the effect is a slight smoothing of the amplitudes. The radial power spectra were derived by azimuthally averaging the squared Fourier amplitudes in equally spaced wavenumber bins. Statistical uncertainties were calculated as $1/\sqrt{n_s}$ times the azimuthal average, where n_s is the number of amplitude samples comprising the average. To ensure that we were not adding structure by noise filtering, the insignificant wavelet coefficients and scales that had been rejected in the filtering process were summed to make a “noise image.” Power spectra of the noise images showed no systematic trends as a function of spatial wavenumber, which is consistent with uncorrelated “white” noise. In addition, a subregion of the *Spitzer* mosaics that has no detectable emission showed the same power spectrum as the noise images.

2.2. IRAS Sky Survey Atlas Images

We used surface brightness maps at 12, 25, 60, and $100\ \mu\text{m}$ from the IRAS Sky Survey Atlas (ISSA). ISSA maps were produced that covered a $12^\circ \times 12^\circ$ region centered on the *Spitzer* subregions. These maps were corrected for gain and offset variations by comparing with measurements taken with the *Cosmic Background Explorer* (COBE) Diffuse Infrared Background Experiment (DIRBE; Miville-Deschênes & Lagache 2004). Before power spectral estimation, the IRAS data were processed for source removal, noise filtering, and point-spread function (PSF) deconvolution according to the method described by Miville-Deschênes et al. (2002).

TABLE 1
COLORS IN *Spitzer* AND *IRAS* MAPS

λ (μm)	$I_\lambda/I_{100\mu\text{m}}$ ^a
8.....	0.039 ± 0.005
12.....	0.029 ± 0.005
24.....	0.041 ± 0.005
25.....	0.048 ± 0.003
60.....	0.315 ± 0.003

^a Slope of linear fit to the surface brightness I_λ as a function of I_{100} , with formal fit errors.

3. RESULTS

3.1. *Spitzer* and *IRAS* colors

Table 1 lists mean surface brightness ratios $I_\lambda/I_{100\mu\text{m}}$ between the *Spitzer* and *IRAS* data. The point-source-subtracted *Spitzer* maps were convolved with the *IRAS* beam and resampled onto the ISSA grid. Linear fits of I_λ as a function of $I_{100\mu\text{m}}$ were performed. The slopes and their errors are reported in Table 1. For most wavelengths, the data were well correlated with $I_{100\mu\text{m}}$. After processing, the MIPS $70\ \mu\text{m}$ image (Fig. 1f) still showed systematic instrumental features, most notably vertical stripes in the direction of the scan legs. We do not analyze the $70\ \mu\text{m}/100\ \mu\text{m}$ color here, in the expectation of improved processing of the $70\ \mu\text{m}$ data. The *Spitzer*-derived spectral energy distribution of the cirrus will be discussed more fully in a future paper.

3.2. Spatial Power Spectrum

Figure 2 displays the spatial power spectra of emission in the fields shown in Figure 1. In each of the three *Spitzer* data sets (IRAC $8\ \mu\text{m}$, MIPS 24 and $70\ \mu\text{m}$), point-source subtraction and noise filtering had an obvious effect on the power spectra. Both processing steps removed a mostly flat “white” noise component. The benefits of point-source removal were most pronounced in the IRAC $8\ \mu\text{m}$ data, while noise filtering greatly improved the linearity of the spectra (in log-log plots) in all three fields.

Power-law fits ($P = Ak^{-\beta}$) to the point-source-removed, noise-filtered spectra are superimposed on the data in Figure 2. The 24 and $70\ \mu\text{m}$ fits gave the same result within the formal fit errors: $\beta_{24\mu\text{m}} = -(3.52 \pm 0.01)$ and $\beta_{70\mu\text{m}} = -(3.48 \pm 0.04)$. In log-log plots, the $24\ \mu\text{m}$ spectrum did not deviate from a straight line for almost 2 decades of spatial frequency, down to the spatial resolution of $\sim 5''$. At the ~ 400 pc distance of the emitting material, this is equivalent to a size scale of ~ 0.01 pc.

In contrast, the $8\ \mu\text{m}$ image had a power spectrum over the same spatial scales that was flatter by 0.4 ($\beta_{8\mu\text{m}} = -[3.13 \pm 0.03]$), indicating more power at small scales than the other two images. A bump in the $8\ \mu\text{m}$ power spectrum at a high wavenumber was probably caused by incomplete source subtraction. Some sources were clearly not pointlike, and subtracting a scaled PSF added high-frequency structure. Unfortunately, this occurred where the IRAC $8\ \mu\text{m}$ image might have provided additional information on the structure at the smallest scales.

We extended the power spectrum of our $24\ \mu\text{m}$ field to large scales using the power spectrum of the *IRAS* map that includes it. Figure 3 shows a comparison of the MIPS $24\ \mu\text{m}$ power spectrum with that of an ISSA $25\ \mu\text{m}$ image that includes the same field. The $25\ \mu\text{m}$ data were normalized (multiplied by a

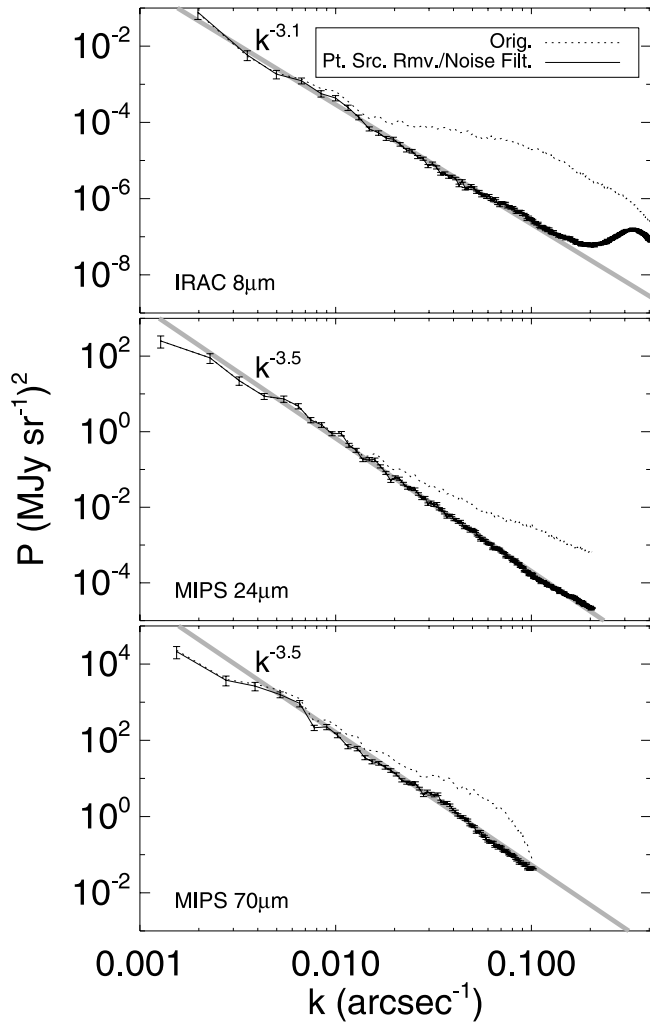


FIG. 2.—Spatial power spectra of emission toward the *Spitzer* fields in Fig. 1: *top*, IRAC 8 μm ; *middle*, MIPS 24 μm ; *bottom*, MIPS 70 μm . Spectra correspond to the two stages of image processing depicted in Fig. 1: original post-BCD mosaic (*dotted lines*), and point-source removed, noise-filtered (*solid lines*). Power-law fits to the point-source-removed, noise-filtered data are superimposed as gray lines and are labeled on the graphs. Statistical error bars are plotted for the point-source-removed, noise-filtered measurements.

constant) to match the 24 μm spectrum in the overlap region and all data points were rebinned for clarity—except for the low- k data, each plot symbol is an average over more than one radial point. The 25 μm power spectrum was fitted by a power law with $\beta_{25\mu\text{m}} = -(2.63 \pm 0.02)$, which is shallower than the 24 μm spectrum by ~ 1 . Our data suggest that there is a transition in the power-law exponent from -2.6 to -3.5 somewhere in the wavenumber range $2 \times 10^{-3} \text{ arcsec}^{-1} < k < 4 \times 10^{-3} \text{ arcsec}^{-1}$. This also seems to occur in the 70 μm data. If the decrease in slope is real, then it is comparable to the bend in the power spectrum of H I seen by Elmegreen et al. (2001) in the Large Magellanic Cloud (LMC), where the spectral exponent also decreased by ~ 1 from low to high k . This is predicted to occur when the transverse size of an image is greater than the line-of-sight depth d_{LOS} of the emitting medium. More precisely, the transition occurs at wavenumber $k = 1/2d_{\text{LOS}}$ (for theoretical and numerical support for this argument, see Lazarian & Pogosyan 2000 and Miville-Deschênes et al. 2003b). Under this hypothesis, we estimated d_{LOS} for the 25 and 24 μm emitting dust cloud. Assume that the transition occurs at $k_{\text{trans}} = 0.003 \text{ arcsec}^{-1}$, or 1.54 pc^{-1} if

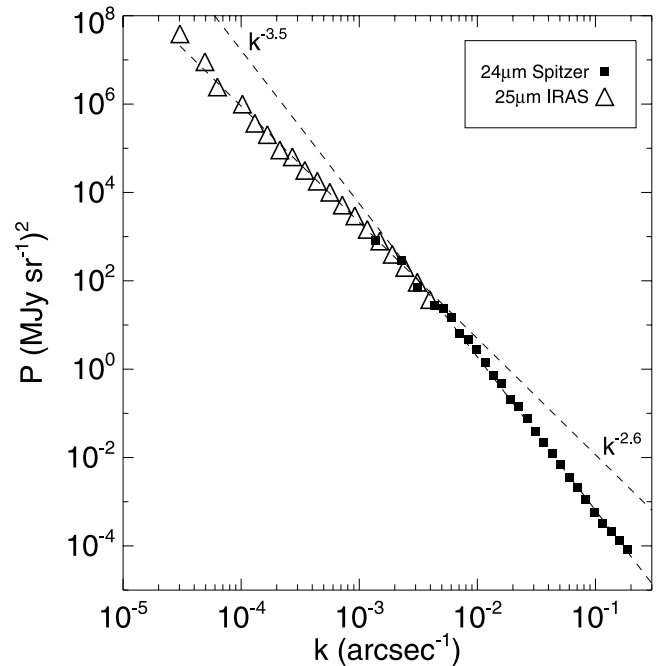


FIG. 3.—Spatial power spectra at 25 μm (*open triangles*; IRAS) and 24 μm (*filled squares*; *Spitzer*) for the field encompassing the images displayed in Fig. 1. Both spectra have been point-source-removed and noise-filtered, albeit with different methods (see § 2). The 25 μm spectrum has been normalized to intersect the 24 μm spectrum. The data have been rebinned in equally spaced logarithmic intervals for clarity. Separate power-law fits are superimposed as dashed lines on the two spectra and are labeled on the graph. We do not plot statistical error bars, since they would be smaller than the symbols.

the distance is 400 pc. Thus, $d_{\text{LOS}} = 1/2k_{\text{trans}} = 0.3 \text{ pc}$. Without invoking distance, we can use the angular size of our map Θ_{map} and the transition wavenumber to estimate the size-to-thickness ratio of the medium $L/d_{\text{LOS}} = 2\Theta_{\text{map}}k_{\text{trans}}$. Taking $\Theta_{\text{map}} = 0.3$ (i.e., the size of the 24 μm image used to compute the high- k power spectrum), $L/d_{\text{LOS}} = 6.5$. This is probably a lower limit, since the emission continues beyond the edges of the map.

4. DISCUSSION

The *Spitzer* 24 and 70 μm surface brightness maps of the Gum Nebula have the same power spectral index, $\beta \approx -3.5$. The 24 μm data in particular conform well to a -3.5 power law down to the spatial resolution of $\sim 5''$, which is equivalent to a size scale of $\sim 0.01 \text{ pc}$ at the estimated distance of $\sim 400 \text{ pc}$. Thus, *the self-similar structure of the 24 μm emission continues to milliparsec scales*. To properly understand the relationship between the emission and the column density, we need to model the variations in grain heating and emissivity as a function of density, extinction, and distance from UV sources. Nevertheless, these β estimates that we have derived for the mid-infrared dust surface brightness are close to the value -3.6 reported for the density and velocity fields of H I in emission in the Galaxy and the LMC (see Miville-Deschênes et al. 2003a and Elmegreen et al. 2001, respectively). A spatial power-spectrum index of -3.5 is also close to the prediction $\beta = -11/3$, based on the Kolmogorov (1941) incompressible turbulence theory. In contrast, the velocity-integrated emission from dense molecular gas typically yields values of $\beta \sim -2.8$ (Stutzki et al. 1998; Bensch et al. 2001; Padoan et al. 2004).

Our power spectral analysis may have enabled us to access the depth of 24 μm emitting material along the line of sight

$d_{\text{LOS}} \approx 0.3$ pc. The steepening of the power spectrum from $\beta_{2\text{D}}$ to $\beta_{3\text{D}} \approx \beta_{2\text{D}} - 1$ (in our case, from -2.6 to -3.5) is predicted to occur when the size of the map is larger than d_{LOS} (Miville-Deschênes et al. 2003b). At small wavenumbers the image power spectrum reverts to that of a two-dimensional field, i.e., the projected three-dimensional volume statistics are equivalent to those of a two-dimensional slice, and the power spectrum flattens.⁶ The two/three-dimensional transition has been observed before in the LMC (Elmegreen et al. 2001), but this is the first example in the Milky Way.

What is the physical significance of the 0.3 pc emitting layer thickness? There are two possibilities that depend on the excitation of dust grains into emission in the 24 μm band. If the emission is dominated by dark regions, then d_{LOS} could be the average “skin depth” for penetration of UV photons or the depth beyond which the abundance of emitters decreases drastically. The skin-depth effect should be even more apparent in the 8 μm emission, but less apparent in the 70 μm emission.

If, on the other hand, the emission comes from mostly diffuse regions with $A_V \lesssim 1$ mag, then UV photons permeate the entire cloud, and d_{LOS} is the average thickness of the Gum

Nebula shell itself. While opaque lines of sight do exist in the Gum Nebula (e.g., the cometary globules studied by Sridharan 1992), on $\sim 2'$ scales our field has only moderate extinction, $A_V < 1.1$ mag (derived from the brightest ^{12}CO contour of Yamaguchi et al. 1999). Furthermore, the 70 μm power spectrum also shows evidence of a break at $k = 0.003$ arcsec $^{-1}$, implying that $d_{\text{LOS}} = 0.3$ pc is independent of excitation. The 24 and 70 μm data show only one scale in which the two/three-dimensional transition occurs.

It would not be surprising if the 24 μm size-to-thickness ratio $L/d_{\text{LOS}} \gtrsim 6.5$ applied not only to the small portion of the Gum Nebula that we have observed, but to the diffuse medium of the Galaxy in general. In an H I survey of the cold neutral medium, Heiles & Troland (2003) demonstrated that clouds are “sheet-like,” with size-to-thickness ratios of up to 280. Far from being unusual, the two/three-dimensional power-spectrum break that we see may be a normal feature of large spatial dynamic range observations of the local cold, neutral ISM.

This work is based on observations made with the *Spitzer Space Telescope*, which is operated by the Jet Propulsion Laboratory, California Institute of Technology, under NASA contract 1407. Support for this work was provided by NASA through an award issued by JPL/Caltech. We thank the referee, Paolo Padoan, for his comments that improved the manuscript.

⁶ An alternative interpretation holds that the break in the spectral index is caused by the lack of self-similarity in the three-dimensional turbulence above the scale where the system becomes two-dimensional (Padoan et al. 2001). Even under this interpretation, however, the observed break would mark the thickness of the system.

REFERENCES

- Bensch, F., Stutzki, J., & Ossenkopf, V. 2001, *A&A*, 366, 636
 Chandrasekhar, S. 1949, *ApJ*, 110, 329
 Diolaiti, E., Bendinelli, O., Bonaccini, D., Close, L. M., Currie, D. G., & Parmeggiani, G. 2000a, *Proc. SPIE* 4007, 879
 ———. 2000b, *A&AS*, 147, 335
 Elmegreen, B., Kim, S., & Stavely-Smith, L. 2001, *ApJ*, 548, 749
 Falgarone, E., Hily-Blant, P., & Levrier, F. 2004, *Ap&SS*, in press
 Fazio, G., et al. 2004, *ApJS*, 154, 10
 Gautier, T. N., III, Boulanger, F., Pérault, M., & Puget, J.-L. 1992, *AJ*, 103, 1313
 Hartley, M., Manchester, R. N., Smith, R. M., Tritton, S. B., & Goss, W. M. 1986, *A&AS*, 63, 27
 Hegmann, M., & Kegel, W. H. 2000, *A&A*, 359, 405
 ———. 2003, *MNRAS*, 342, 453
 Heiles, C., & Troland, T. H. 2003, *ApJ*, 586, 1067
 Herbstmeier, U., et al. 1998, *A&A*, 332, 739
 Joulain, K., Falgarone, E., Des Forêts, G. P., & Flower, D. 1998, *A&A*, 340, 241
 Juvela, M., & Padoan, P. 2003, *A&A*, 397, 201
 Kolmogorov, A. N. 1941, *Dokl. Akad. Nauk SSSR*, 30, 9
 Lazarian, A., & Pogosyan, D. 2000, *ApJ*, 537, 720
 MacLow, M.-M., & Klessen, R. S. 2004, *Rev. Mod. Phys.*, 76, 125
 Miville-Deschênes, M.-A., Joncas, G., Falgarone, E., & Boulanger, F. 2003a, *A&A*, 411, 109
 Miville-Deschênes, M.-A., & Lagache, G. 2004, *ApJ*, submitted
 Miville-Deschênes, M.-A., Lagache, G., & Puget, J.-L. 2002, *A&A*, 393, 749
 Miville-Deschênes, M.-A., Levrier, F., & Falgarone, E. 2003b, *ApJ*, 593, 831
 Ossenkopf, V. 2002, *A&A*, 391, 295
 Padoan, P., Jimenez, R., Juvela, M., & Nordlund, Å. 2004, *ApJ*, 604, L49
 Padoan, P., Juvela, M., Bally, J., & Nordlund, Å. 1998, *ApJ*, 504, 300
 Padoan, P., Kim, S., Goodman, A., & Stavely-Smith, L. 2001, *ApJ*, 555, L33
 Rieke, G., et al. 2004, *ApJS*, 154, 25
 Röllig, M., Hegmann, M., & Kegel, W. H. 2002, *A&A*, 392, 1081
 Spaans, M. 1996, *A&A*, 307, 271
 Sridharan, T. K. 1992, *J. Astrophys. Astron.*, 13, 217
 Starck, J.-L., & Murtagh, F. 1998, *PASP*, 110, 193
 Stutzki, J., Bensch, F., Heithausen, A., Ossenkopf, V., & Zielinsky, M. 1998, *A&A*, 336, 697
 Werner, M. W., et al. 2004, *ApJS*, 154, 1
 Woermann, B., Gaylard, M. J., & Otrupcek, R. 2001, *MNRAS*, 325, 1213
 Yamaguchi, N., et al. 1999, *PASJ*, 51, 765

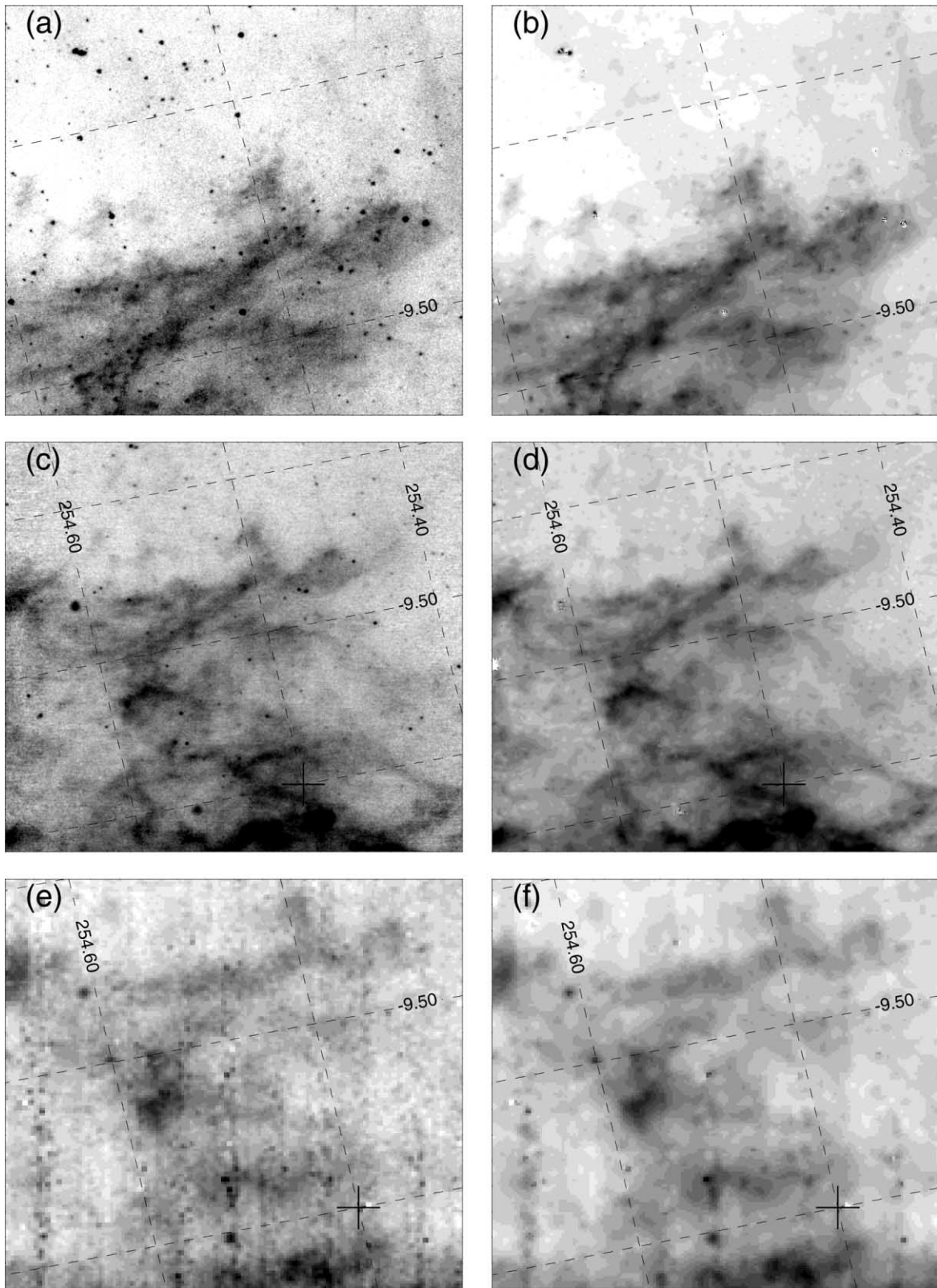


FIG. 1.—*Spitzer* surface brightness maps used for power spectral analysis. The field includes a molecular cloud associated with the Gum Nebula. (a) and (b): IRAC $8\ \mu\text{m}$ gray levels range from 0.28 (white) to $0.33\ \text{MJy sr}^{-1}$ (black). (c) and (d): MIPS $24\ \mu\text{m}$ gray levels range from 19.1 to $20.8\ \text{MJy sr}^{-1}$. (e) and (f): MIPS $70\ \mu\text{m}$ gray levels range from 20 to $490\ \text{MJy sr}^{-1}$. (a), (c), and (e): Original post-BCD mosaic images. (b), (d), and (f): Results of point-source subtraction and noise filtering (see text) applied to the left-column images. Each map has the same grid of Galactic coordinates superimposed (grid lines are separated by $0''.1$). A cross in panels (c) through (f) shows the position of cloud DC 254.5–9.6 (Hartley et al. 1986).

ERRATUM: “STRUCTURE AND COLORS OF DIFFUSE EMISSION IN THE *SPITZER* GALACTIC FIRST LOOK SURVEY” (ApJS, 154, 281 [2004])

JAMES G. INGALLS, M.-A. MIVILLE-DESCHÊNES, WILLIAM T. REACH, A. NORIEGA-CRESPO, SEAN J. CAREY,
 F. BOULANGER, S. R. STOLOVY, DEBORAH L. PADGETT, M. J. BURGDORF, S. B. FAJARDO-ACOSTA,
 W. J. GLACCUM, G. HELOU, D. W. HOARD, J. KARR, J. O’LINGER, L. M. REBULL,
 J. RHO, J. R. STAUFFER, AND S. WACHTER

We have discovered an error in the scaling of our IRAC 8 μm and MIPS 70 μm data, which affected the caption for Figure 1 and the vertical axis scales for Figure 2.

The original units in the images displayed in Figure 1 were MJy sr^{-1} for 8 μm and $\mu\text{Jy arcsec}^{-2}$ for MIPS 24 and 70 μm . We incorrectly multiplied our IRAC data by 0.0425 (the conversion from $\mu\text{Jy arcsec}^{-2}$ to MJy sr^{-1}), but neglected to multiply our MIPS 70 μm data by that factor. (MIPS 24 μm data were scaled correctly.) Thus, contrary to the caption of Figure 1, the gray levels for panels (a) and (b) actually range from 6.7 to 7.8 MJy sr^{-1} , and the gray levels for panels (e) and (f) actually range from 0.85 to 20.8 MJy sr^{-1} .

The power spectra in Figure 2 should have been normalized such that the integral over the spectrum equals the mean square image surface brightness. In the original paper, however, the IRAC power spectrum was incorrectly multiplied by $(0.0425)^2$, whereas the MIPS 70 μm spectrum should have been multiplied by this factor but was not. We correct this in a revised version of Figure 2 included here.

We thank Rick Arendt for calling our attention to this error.

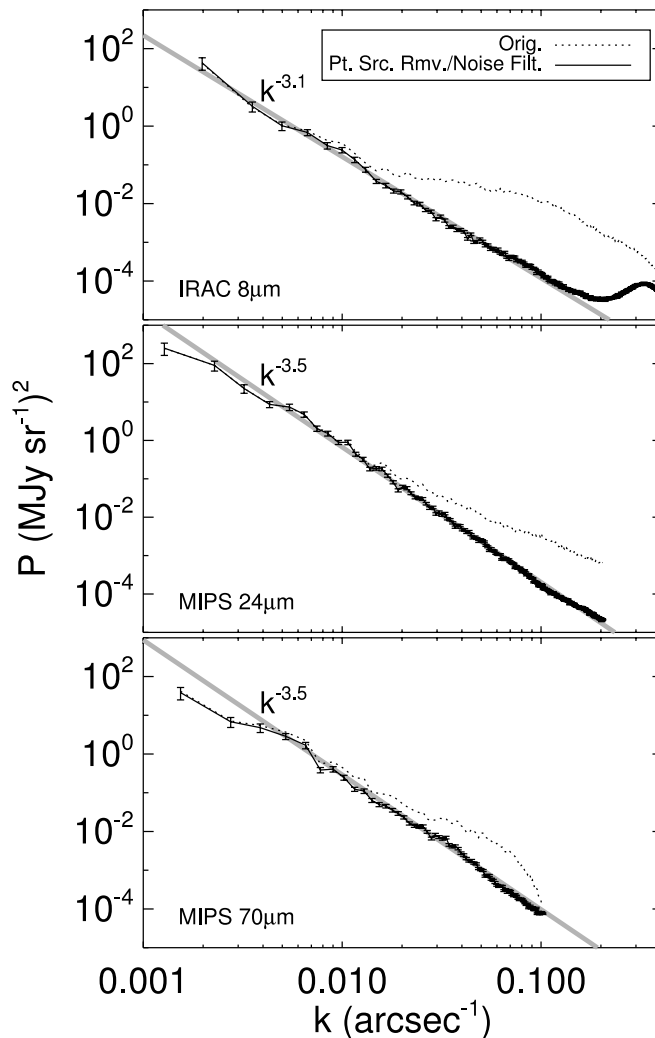


FIG. 2.— Spatial power spectra of emission toward the *Spitzer* fields in Fig. 1: *top*, IRAC 8 μm ; *middle*, MIPS 24 μm ; *bottom*, MIPS 70 μm . Spectra correspond to the two stages of image processing depicted in Fig. 1: original post-BCD mosaic (*dotted lines*), and point-source removed, noise-filtered (*solid lines*). Power-law fits to the point-source-removed, noise-filtered data are superimposed as gray lines and are labeled on the graphs. Statistical error bars are plotted for the point-source-removed, noise-filtered measurements.

This figure replaces Fig. 2 of the original manuscript. The only change from the original is that the power spectrum for IRAC 8 μm has been divided by $(0.0425)^2$, whereas that for MIPS 70 μm has been multiplied by that factor. The vertical axis scales have also been adjusted so that they are the same for each panel.